Initial crustal thickness geometry controls on the extension in a back arc domain: Case of the Gulf of Corinth

Laetitia Le Pourhiet[1]
Institut Français du Pétrole, Rueil Malmaison, France

Evgenii Burov
Laboratoire de Tectonique, Université Pierre et Marie Curie, Paris, France

Isabelle Moretti
Institut Français du Pétrole, Rueil Malmaison, France

Received 28 June 2002; revised 23 October 2002; accepted 17 April 2003; published 15 July 2003.

[1] Since 60 Myr, Peloponnesus and continental Greece have been affected by the Hellenidean compressional and the Aegean extensional phases. This complex evolution resulted in development of a strongly inhomogeneous crust in the Gulf of Corinth region. To study this area, we use a large strain thermomechanical numerical code PARAVOZ previously used for a number of similar problems such as rift evolution. Yet, instead of varying boundary and initial conditions applied to a plane-layered model, we use available geophysical constraints on the actual deep structure of the lithosphere to test its different possible initial structures. By varying the position of the initial crustal heterogeneity versus the position of the lithospheric slab, we are able to explain the origin of the internal structures and the kinematics of the Gulf of Corinth. The results suggest that the development of shear zones in the lower crust is favored by the gravitational collapse of the thicker part of the crust, whereas the geometry and the kinematics of these shear zones are controlled by the position of the edge of the slab. Asymmetry is seen in cases when a horizontal shift exists between the edge of the slab and the thicker part of the crust. Our model explains the differences between the northern shore and the southern shore as well as the east west variations observed in the Gulf of Corinth. *INDEX TERMS:* 8109 Tectonophysics: Continental tectonics—extensional (0905); 8020 Structural Geology: Mechanics; 3210 Mathematical Geophysics: Modeling; *KEYWORDS:* Gulf of Corinth, rifting, strain localization, back arc extension, Greece. **Citation:** Le Pourhiet, L., E. Burov, and I. Moretti, Initial crustal thickness geometry controls on the extension in a back arc domain: Case of the Gulf of Corinth, *Tectonics*, *22*(4), 1032, doi:10.1029/2002TC001433, 2003.

[1]Also at Laboratoire de Tectonique, Université Pierre et Marie Curie, Paris, France..

0278-7407/03/2002TC001433$12.00

1. Introduction

1.1. Regional Setting

[2] The Gulf of Corinth is located between Peloponnesus and continental Greece on the Aegean plate. It is limited to the south by the Hellenic trench (Figure1) and to the north by the North Anatolian fault. The subduction of the eastern Mediterranean oceanic crust beneath the Aegean domain started 60 Myr ago, leading to the superposition of different nappes (Figure 1). Since Miocene times the central part of the Aegean domain has undergone large extension that has lead to the exhumation of the metamorphic rocks previously involved in the compression [*Gautier et al.*, 1999] (Figure 1). During the Miocene phase of extension, the direction of the lineation of extension is regionally, with azimuth ranging from N30° to N50°. The age of high-pressure metamorphism decreases in the southward direction, which indicates that the large extension in the Aegean Sea was most probably caused by the southward migration of the trench [*Jolivet*, 2001; *Jolivet et al.*, 1994]. In this general framework, the present-day extensional phase resulted in formation of a system of grabens on both sides of the Aegean Sea (Evvia, Corinth, Turkey), developed in a highly heterogeneous continental lithosphere.

1.2. Geometry of the Gulf of Corinth

[3] The approximate azimuthal orientation of the axis of the Gulf of Corinth is N120°, whereas the border faults are N90° oriented (Figure 2). The gulf is wider to the east (40 km wide at Corinth isthmus) than to the west (3 km wide at Rio). The water depth is 900 m to the east and only 70 m at Rio. The sedimentary thickness in the gulf also decreases from the east (2.5 km) to the west (1.5 km). The basement is composed of Mesozoic nappes that took place during the formation of the Hellenides. South of Corinth, near Pheneos, the lowest Hellenic nappe outcrops in a tectonic window and is characterized by a blue schist facies [*Xypolias and Doustos*, 2000]. Field and microstructural observations show that the direction of the lineations of extension range between N30° and N50° and that shear sense is directed top-to-the-north at the

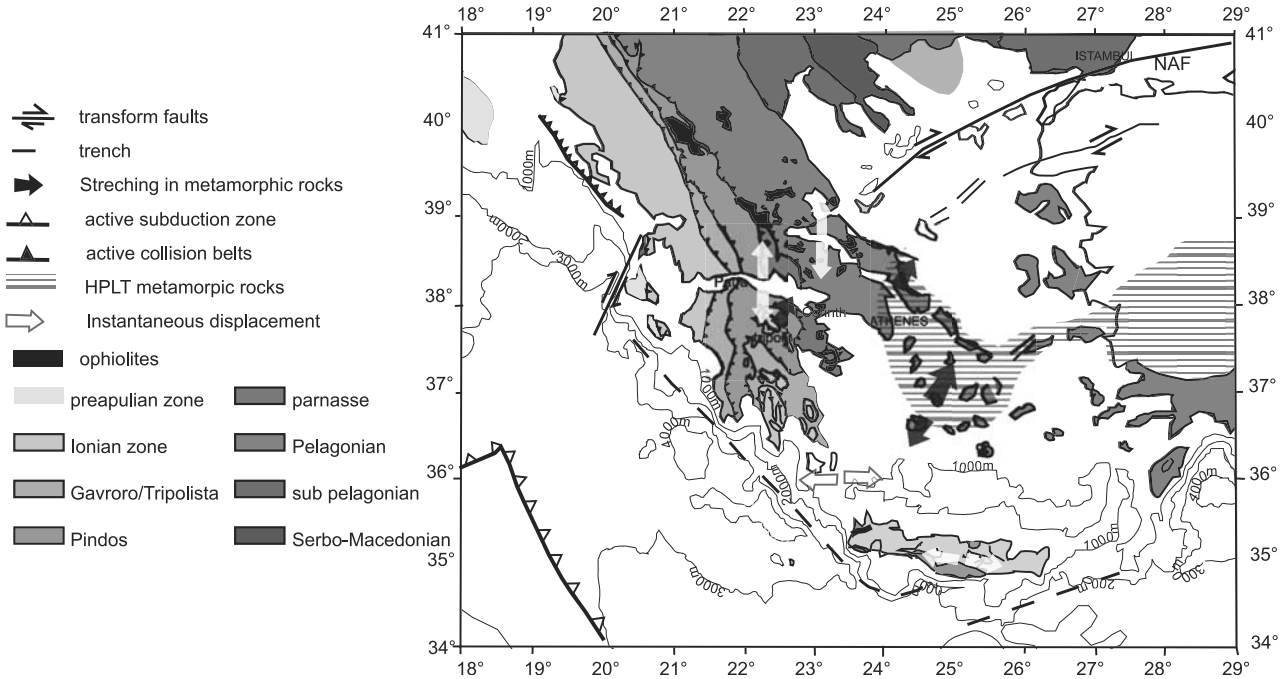

Figure 1. Geological and structural map of the Aegean area. Hellenic nappes [after *Aubouin et al.*, 1970; *Jacobshagen et al.*, 1978], metamorphic high-pressure/low-temperature metamorphic grade (HPLT) exhumed rocks (shaded on the map) (after *Gautier et al.* [1999] and *Jolivet et al.* [1994] for Aegean Sea, *Trotet* [2000] for Peloponnesus, and *Gautier and Brun* [1994] and *Gautier et al.* [1999] for Evvia Island).

boundary of the window (B. Ghorbal and L. Jolivet, personal communication, 2002). Even if the deformation has not yet been dated, this structural information has a strong affinity with the Miocene phase of extension. Moreover, no evidence of continuity between the ductile shear zone and the recent brittle deformation has been found on the field.

1.2.1. Synrift Sedimentation

[4] The outcropping faults in the Aigion area dip at angles ranging from 55° to 70° to the north and have

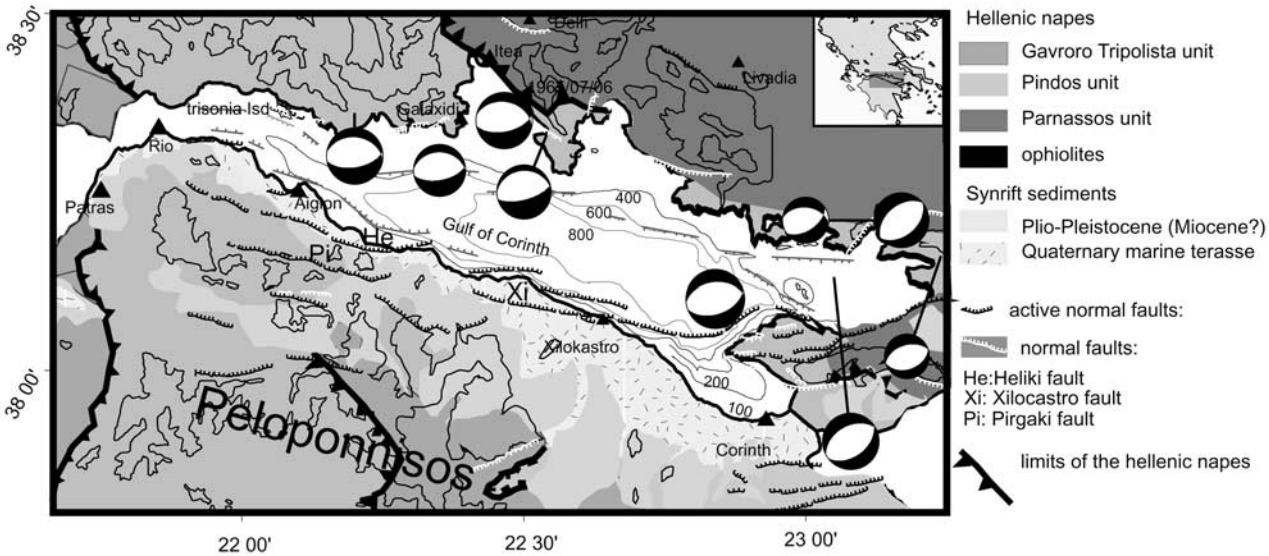

Figure 2. Geological and structural map of the Gulf of Corinth. Focal mechanisms of the main earthquakes [after *Rigo et al.*, 1996] show that the recent extension is N00°. The lineations of extension in the metamorphic window of Pheneos (stripped on the map) trend N30–50° [*Ghorbal*, 2002].

accumulated a vertical offset of more than 500 m in less than 200 kyr [*Ghisetti et al.*, 2001; *Micarelli et al.*, 2002]. On the southern shore, the first synrift deposits reach an elevation of 2 km. Recent marine terraces (Figure 2) also indicate that uplift is still active over the southern shore. *Armijo et al.* [1996] calculated an uplift of 2 mm yr^{-1} for the last 350 kyr using the marine terraces east of the town of Xylocastro. Recent data in the area of Aigion indicate an uplift of 1.5 mm yr^{-1} on the Helike fault [*Pantosti et al.*, 2001]. The synrift sediments of the southern coast have been studied by various authors who generally propose a two-phase model [e.g., *Ori*, 1989]. During the first phase (Pliocene), the deposits were distributed on a wide area, with facies varying from lacustrine to alluvial fan deltas. During the second phase, the well-developed Gilbert fan deltas indicate higher subsidence rate and sedimentary inflow than during the first phase. Moreover, the deposits are located on more restricted area. On the northern shore, normal faults are also present. Yet, there is no synrift sediment thus they are poorly studied. However, marine data indicate that the current depocenter in the western part of the gulf is located near the northern shore at the level of the Trisonia Island [*Stefatos et al.*, 2002a, 2002b]. In the eastern part of the gulf, the commercial seismic data reprocessed by *Clément* [2000] show that the depocenter was first located on the northern shore and then migrated southward [*Moretti et al.*, 2002].

1.2.2. Geometry of the Crust

[5] The depth map of the Moho (Figure 3a) indicates that crustal thickening is decreasing eastward from 50 km at Patras to 25 km at the Corinth Isthmus. This general observation relates clearly to the Miocene extension in the Aegean Sea. The most important observation is that contrary to what is commonly inferred; the crust is thicker under the basin than beneath its both borders. Actually, this phenomenon is not restricted to the Gulf of Corinth, but represents a regional common feature manifested by N30° short-wavelength undulations of the Moho depth. These undulations have a typical amplitude of 10km and are expected to cause strong gravitational instabilities in the crust. Yet their origin is still an open question. Three hypotheses can be proposed to explain these undulations: (1) remnant Moho variations from the compressional phase, (2) crustal thinning related to previous extensive events such as the Miocene extension in the whole Aegean domain, including the Peloponnesus, or (3) Quaternary features related to the current rifting phase (grabens of Corinth and Evvia).

[6] It is our opinion that the third hypothesis had to be rejected because the trend of the undulations is not parallel to the recent direction of extension (N00°). The first hypothesis may explain why part of the crust is thicker than normal. Still, this hypothesis also has to be rejected because the trend of the undulations and the one observed for the compressional structures around Corinth have no affinity. Therefore the second hypothesis appears to be most realistic for two reasons. First, it may explain the crustal thinning observed south of the Gulf of Corinth as geographically this thinning is exactly located under the metamorphic windows of Pheneos (see section 1.2). Second, the trend of the undulations is identical to the direction of the Miocene extension phase. For these reasons, we will consider that the undulation existed before the current rifting phase in the Gulf of Corinth.

1.2.3. Geometry of the Subducting Slab

[7] The azimuth of the trench changes. It trend along the Peloponnesus varying from N90° along the Crete Island to N00° along the Ionian Islands. The current lithospheric slab geometry can be traced from seismic tomography models [*Spakman et al.*, 1988; *Tibéri*, 2000] and data on deep seismicity [*Tibéri*, 2000] (Figure 3b). The regional heat flow values [*Fytikas and Kolios*, 1979] (Figure 3c) are rather typical for a back arc extensional regime. The distribution of high heat flow anomalies and deep earthquakes correlate together with the bend in the trend of the slab. The tomography cross section (Figure 3b) indicates that the dip angle of the subducting slab changes abruptly. The position of this change (noted A on Figure 3b) is approximately below the Gulf of Corinth. As the accuracy of the position of A is poor and the azimuth of the slab (N150°) differs from the trend of the gulf (N120°), we varied the initial position of point A relatively to the position of the thickened part of the crust in our numerical models.

1.3. Present Activity

[8] The Gulf of Corinth is a seismically very active area where observed vertical and horizontal velocity of displacements is very high for an area encountering extensive strain. GPS data [*Briole et al.*, 1999] show evidence of an east–west contrast. The opening direction is N00. The opening rate decrease eastward from 1.5 cm yr^{-1}, at Rio, to 0.5 cm yr^{-1}, at the level of the isthmus (Figure 3d). In the central and western part of the gulf, clusters of seismicity have been recorded between 5 and 10 km depth [*Rigo et al.*, 1996]. The seismic activity seems to be limited downward along plane dipping 20–30°N. Three large earthquakes have been recorded during the last 10 years. Their epicenters are below of the northern margin of the gulf. Their focal mechanisms indicate a slip along rather low-angle normal faults dipping 30° to 35° to the north [*Lyon Caen et al.*, 2002]. This bottom of the seismogenic zone could be interpreted as the brittle–ductile transition, or alternatively as a newly formed structure [*Sorel*, 2000]. A recently recorded crisis took place between the faults of Helike and Pirgaki. The clusters define a high-angle structure (dipping about 70° to the north), which could be interpreted as the deepest part of the Pirgaki fault (H. Lyon Caen et al., submitted to *Compte Rendus de l'Académie des Sciences*, 2003). This high-angle structure confirms the model of *Rigo et al.* [1996] in which planar faults were rooting at the base of the seismogenic zone (Figure 3e). In contrast, in the eastern part, the faults dip with a rather normal angle at depth (45°–50°) [*Rigo et al.*, 1996].

1.4. Present Approach

[9] The Gulf of Corinth is one of the most extensively studied, but still not well understood, active extensional

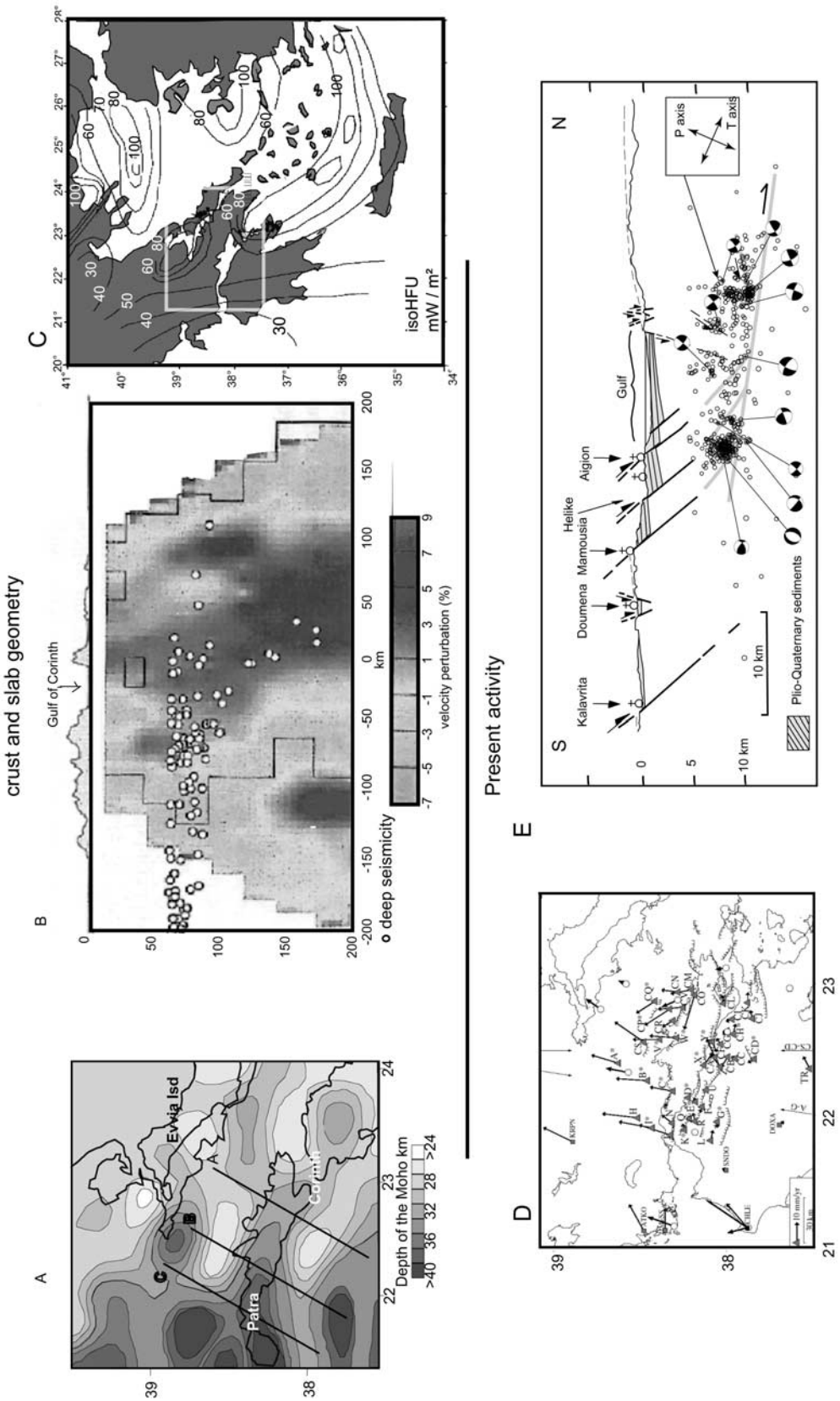

Figure 3. (a) Depth of the Moho deduced from gravimetric data [after *Tiberi*, 2000]. Profiles 1, 2, and 3 on the map correspond in cross sections to initial geometries (cases a, b, and c) used for modeling (see Figure 5). (b) Tomographic cross section and deep seismicity indicating the geometry of the slab under the Gulf of Corinth [after *Tiberi*, 2000]. (c) Regional heat flux [after *Fytikas and Kolios*, 1979]. (d) Horizontal instantaneous displacement deduced from GPS [after *Briole et al.*, 1999]. (e) Shallow seismicity [after *Rigo et al.*, 1996]. The *P* and *T* axes are rotated indicating simple shear stress state. The seismicity is limited downward by a low-angle dipping plane.

Table 1. Parameters for Elastoplasticity

Parameter	Value
λ	3×10^{10} Pa
G	3×10^{10} Pa
C_0	2×10^{7} Pa
ϕ	30°

Table 2. Parameters for Non-Newtonian Viscosity

Phases	n	A, MPa^{-n} s^{-1}	E, kJ mol^{-1}
Continental upper mantle	3	1.00×10^{4}	520
Asthenosphere	3	1.00×10^{4}	520
Crust	3	6.80×10^{-6}	156
Oceanic lithosphere	3	1.00×10^{4}	520

area of the world. There may be some reasons for this: (1) The deepest parts of the gulf in terms of water depth and sediments thickness are located where the extension rate is the lowest (the eastern part). (2) In the western part of the gulf, the graben is located where the crust is the thickest in between two thinned parts of the crust. These contradictions cannot be explained neither by the pure shear model [*McKenzie*, 1972] because the graben is shifted with respect to the area of maximum thinning of the crust, nor by simple shear model [*Wernicke*, 1981] because the depocenters are not migrating in the direction suggested by this model. Because the geological setting in which the so-called quaternary "Rift" of Corinth takes place, is very complex, we decided to use an alternative model approach. Instead of focusing on the boundary conditions and the rheology of the lithosphere, this study aims at demonstrating the importance of the initial geometry on rifting process. We will therefore consider that the current crustal thickness changes are representative of thickness variations before the opening of the Gulf of Corinth (~1.5 Myr) and focus on how the initial geometry of the lithosphere controls (1) the geometry of the newly formed rift and (2) the localization of the extensive strain inside the crust.

2. Experiments

2.1. Numerical Method

[10] We use the finite element code PARAVOZ [*Poliakov et al.*, 1993] derived from the FLAC method [*Cundall*, 1989]. PARAVOZ presents a hybrid finite elements/differences fully explicit time marching Lagrangian algorithm operating in large strain mode. It solves the Newton equations of motion in continuum mechanics formulation fully coupled with the heat transport equation. The algorithm was well tested on many extensional problems [e.g., *Poliakov and Buck*, 1996; *Burov and Poliakov*, 2001]. The description and benchmarks of the algorithm can be found in the abundant FLAC-related literature [e.g., *Cundall*, 1989; *Poliakov et al.*, 1993]. The numerical algorithm allows the faults to form themselves during loading in a self-consistent way. Another advantage of the method is that the geometry of layers can be complex allowing us to test different initial geometries derived from geophysical and field observations. In the code, as in nature, the brittle-ductile transition is not predefined a priori but is evaluated on each time step as a function of the local strain rate, stress and temperature. Thus it is possible to make direct comparisons between the predicted depth and geometry of the brittle-ductile transition and the observed thickness and geometry of the seismogenic crust.

2.2. Rheology and Physical Properties of Rock

[11] Parameters for elastic-plastic behavior are fixed for all materials with parameters indicated in Table 1. Parameters for mantle and oceanic lithosphere are derived from olivine's creep behavior, while continental crust follows the quartz creep law (Table 2).

[12] The brittle-ductile transition inside the crust depends on local temperature, stress and strain rate and is therefore dynamically updated during computations. No specific interface is initially set in the model between the lower and upper crust and a mean density at normal pressure is used for the whole crust (Table 3).

[13] Softening used for the brittle part follows the rather weak cohesion softening law [*Lavier et al.*, 1999]. This law reflects natural cohesion loss due to important frictional sliding and allows us to localize plastic strain on one fault after it was formed. This assumption is consistent with the geometry of the faults in Corinth and Evvia rifted basins where most of the deformation is accommodated on major faults.

2.3. Boundary Conditions

[14] Boundary conditions reflect regional extensional settings (Figure 4a) combined with slab pull (Figure 4b). Hydrostatic boundary conditions are used at the bottom of the model, the upper surface is stress free, the horizontal velocity of the right-lateral boundary is fixed to zero while the divergent velocity, Vx, is applied to the left-lateral boundary. To simulate slab pull, a vertical velocity of 1 cm yr^{-1} is applied at the bottom of the model, on 60 km from the edge of the slab in a southward direction (Figure 4b). For all models, Vx is fixed at 2 cm yr^{-1}. The boundary conditions for the thermal part are shown in Figure 4c. They consist of

Table 3. Density and Thermal Conductivity of Phases

Phases	Thermal Conditions, W m^{-1} deg^{-1}	Density, kg m^{-3}
Continental upper mantle	3.5	3300
Asthenosphere	3.5	3280
Crust	2.5	2800
Oceanic lithosphere	3.5	3300

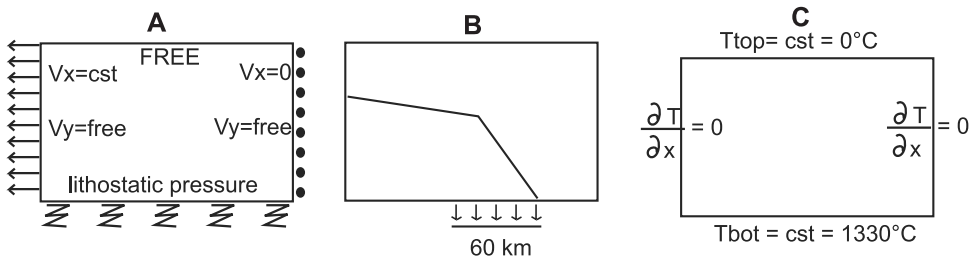

Figure 4. Boundary conditions. (a) Extensional setting with a fixed northern border and a fixed velocity applied on the southern border. Hydrostatic conditions are applied at the bottom while the top surface is free. (b) Slab pull is applied at the bottom of the model on the last 60 km of the lithospheric slab. (c) Temperature is constant at top and bottom. Null flux is applied on both sides.

fixed temperature at both bottom and top and null thermal flux on both sides of the model.

2.4. Initial State

[15] The interpretations of the variations in crustal thickness have been previously discussed (see section 1.1). The following numerical experiments take these variations into account as well as the presence and the position of the subducting slab. Thus complex initial states have been used to evaluate the possible interactions between both these features and their influence on the style of deformation during the last million years in the Gulf of Corinth.

3. Description of the Experiments

[16] In this study, we basically test three major initial possible geometries (Figures 5a to 5c), which correspond to possible positions of the slab related to the initial heterogeneity of the crust when the last phase of rifting in the Gulf of Corinth started.

3.1. Preliminary Tests

[17] Prior to testing of these main hypotheses, we first conducted a number of preliminary experiments aimed at estimating the model's sensitivity to various parameters. During these experiments, the rheological parameters were fixed as shown in Tables 1 and 2, and we varied the boundary conditions (symmetric or asymmetric lateral velocity) and the initial geotherms. The first group of the preliminary experiments aimed at determinate the influence of boundary conditions on the strain pattern. They showed that the asymmetry in lateral boundary conditions produces second order effect on the localization of initiation of the brittle deformation (faulting) but has negligible influence on the deformation of deeper crustal interfaces, which is obviously dominated by gravity driven deformation mechanisms.

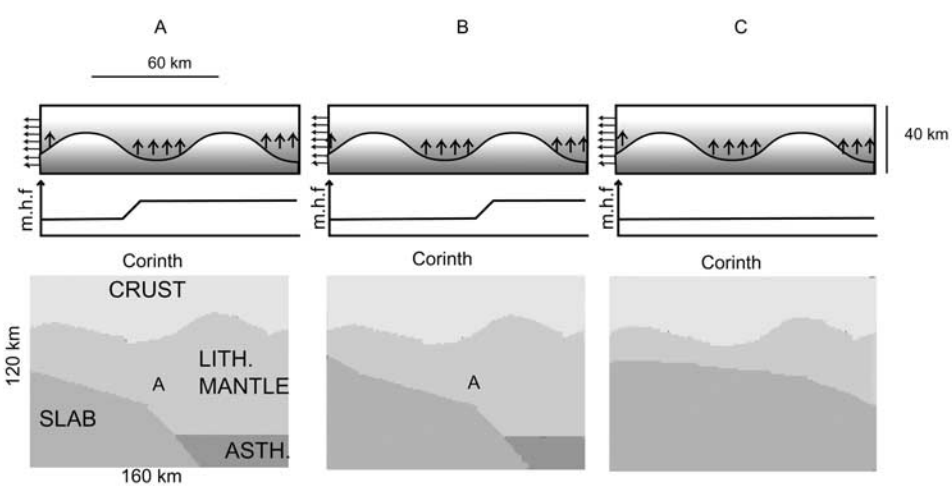

Figure 5. Initial geometries and predicted heat flow at the base of the continental crust Point A is located where the dip of the lithospheric slab changes. (a) High and laterally homogenous heat flow at the base of the continental crust, the point A located under thickened continental crust; (b) laterally inhomogeneous heat flow at the base of the continental crust, the point A shifted from the thickened part of continental crust; and (c) low and homogeneous heat flow at the base of the crust, the slab is flat, there's no convective thermal anomaly in the asthenospheric mantle.

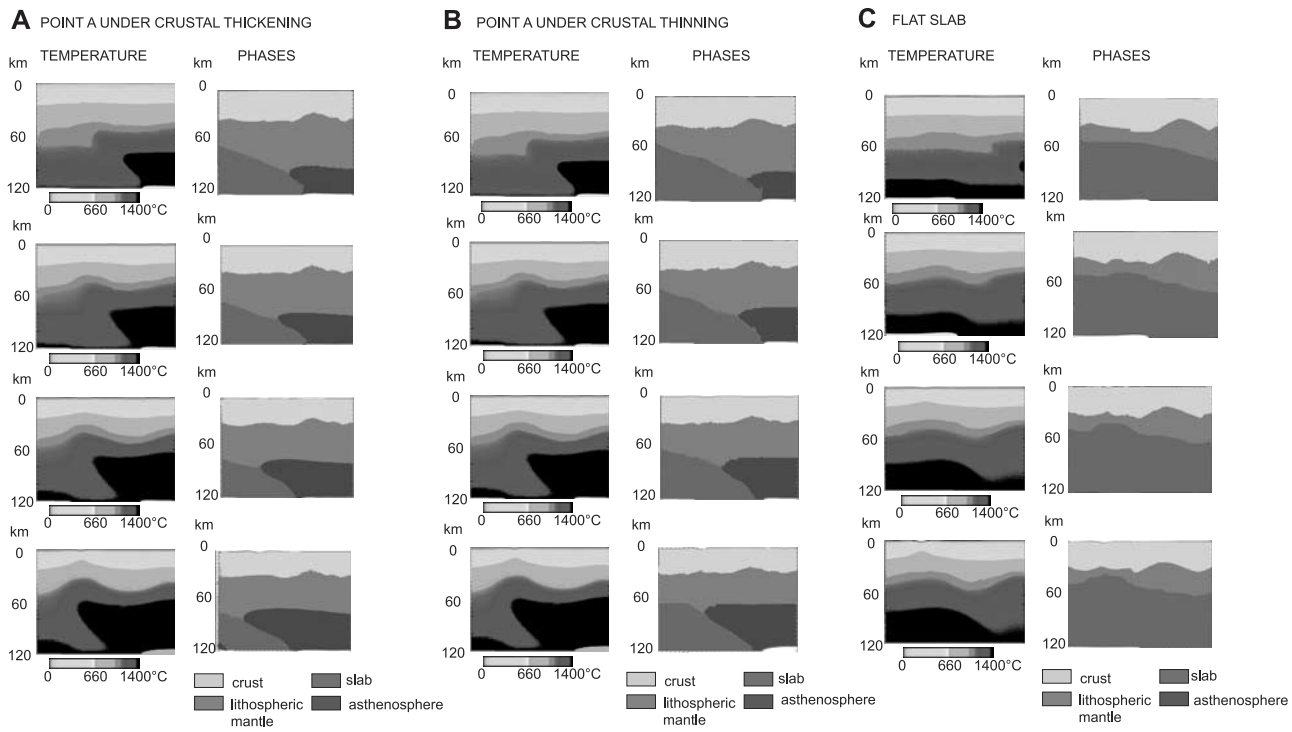

Figure 6. (a), (b), and (c) Two-dimensional distribution of temperature and geometry of the structure for cases presented in Figures 5a, 5b, and 5c, respectively.

[18] Since the content of radiogenic heat-producing elements in the upper crust is difficult to estimate, the initial thermotectonic age (as defined, e.g., by *Burov and Diament* [1995]) is naturally subject to great uncertainties. For this reason we make a second group of preliminary experiments that aims at determinate this parameter for the case of the gulf of Corinth. Thus we varied the thermotectonic age from 50 to 300 Myr. The test for a thermotectonic age of 50 Myr provides the best fit to the observed depth of the brittle-ductile transition [*Rigo et al.*, 1996] for the estimated average strain rates in the region [*Briole et al.*, 1999] and the rheology chosen for crust in the experiments. This hypothesis can easily be supported because the upper crustal granites in the Aegean domain are dated at about 20–30 Myr.

3.2. Initial State for Our Study

[19] Figure 5 shows three possible basic initial situations for recent extension in Corinth. The critical point A corresponds to the break in the dip angle of the slab observed in the tomographic data [*Tibéri*, 2000]. Its lateral position with respect to the zone of the maximal crustal thickening may vary according to the profile selected (Figure 3a).

[20] Small-scale mantle convection is expected to take place in the front of the lithospheric slab. This would however depend on initial situations of which three examples are represented in Figure 5. The first one considers point A situated under the thickened part of the crust (Figure 5a). The second one corresponds to the position of point A under the thinned part of the crust (Figure 5b) and the last one assumes a flat slab under the whole crust (Figure 5c). One of the obvious effects of the variation in the lateral position of point A is related to the horizontal size of the contact zone between the hot upwelling asthenosphere and the underlying cold lithosphere.

4. Results and Interpretations

[21] The results of the experiments related to the initial hypotheses illustrated in Figure 5, are shown in Figures 6 and 7. Figure 6 presents the evolution of the geometry of the different units through time, while Figure 7 (top) represents strain rate in the first 40 km though time and Figure 7 (bottom) represents plastic strain in the first 20 km of the model. All these cases (Figures 7a–7c) correspond to the setups presented in Figures 5a–5c, respectively.

4.1. Crustal Deformation: Common Predicted Features and Major Differences

[22] In all experiments, the obtained brittle-ductile transition is located between 5 and 10 km depth (Figure 7, bottom), and this result fits the data of the seismogenic zone obtained by *Rigo et al* [1996].

[23] Also, in all cases, from the early beginning, the plastic (brittle) strain concentrates above the thickened parts of the crust (Figures 7a–7c, bottom). At 200 kyr after the onset of rifting, the plastic strain is already localized preferentially at the southern thickened part of the crust. In our model, the northern thickened part of the crust does not follow the same evolution due to the boundary condition

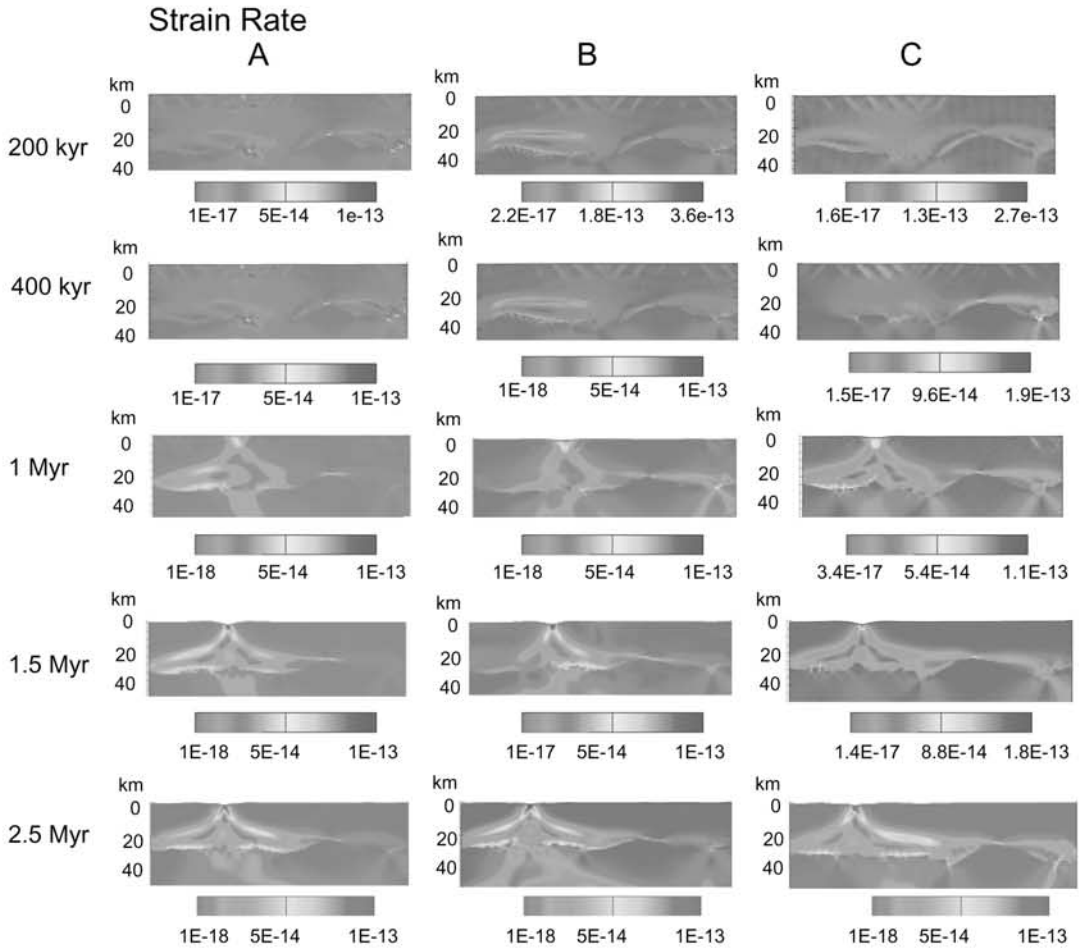
Strain Rate
A
B
C
km
0
20
40
200 kyr
1E-17 5E-14 1e-13
2.2E-17 1.8E-13 3.6e-13
1.6E-17 1.3E-13 2.7e-13
400 kyr
1E-17 5E-14 1E-13
1E-18 5E-14 1E-13
1.5E-17 9.6E-14 1.9E-13
1 Myr
1E-18 5E-14 1E-13
1E-18 5E-14 1E-13
3.4E-17 5.4E-14 1.1E-13
1.5 Myr
1E-18 5E-14 1E-13
1E-17 5E-14 1E-13
1.4E-17 8.8E-14 1.8E-13
2.5 Myr
1E-18 5E-14 1E-13
1E-18 5E-14 1E-13
1E-18 5E-14 1E-13

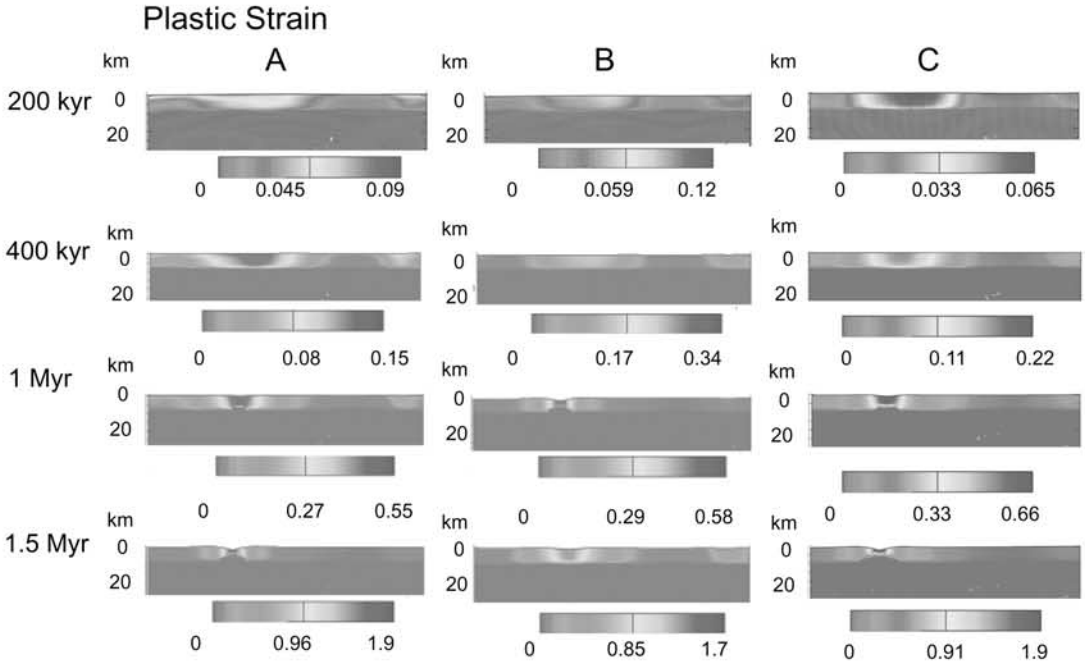
Plastic Strain
A
B
C
km
0
20
200 kyr
0 0.045 0.09
0 0.059 0.12
0 0.033 0.065
400 kyr
0 0.08 0.15
0 0.17 0.34
0 0.11 0.22
1 Myr
0 0.27 0.55
0 0.29 0.58
0 0.33 0.66
1.5 Myr
0 0.96 1.9
0 0.85 1.7
0 0.91 1.9

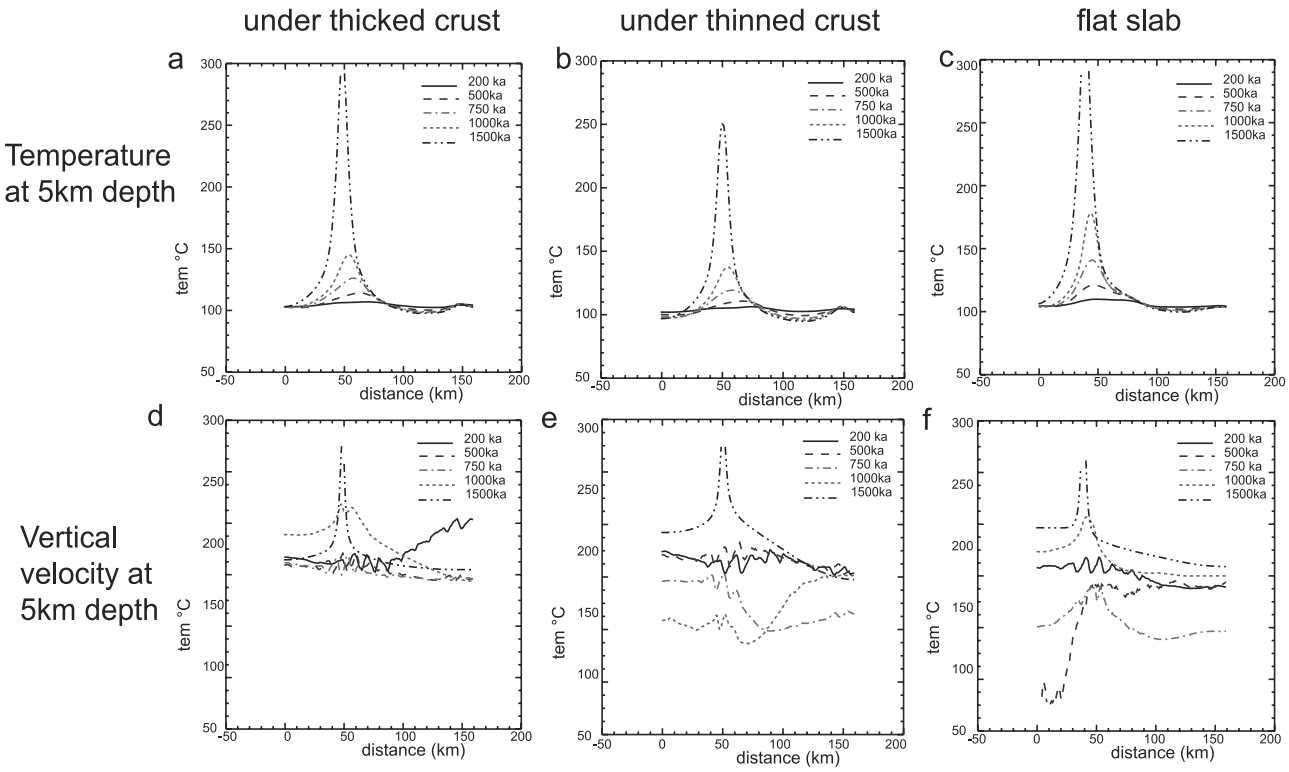

Figure 8. Temperature and vertical velocity at 5 km depth for different time steps. (a, b, c) Temperature. Note the acceleration of heating after 1 Myr for all models. (d, e, f) Vertical velocity. Note the narrowing of the distribution of the high velocity of vertical displacement.

on the right-hand side. This boundary condition effect allows us to compare the evolution of the thick crust under various growth rates and provides a kind of reference between the collapsed zone and the preserved one.

[24] Figure 8 shows the modeled temperature and vertical velocity profiles at 5 km depth for the three experiments. Where crustal collapse occurs (Figure7), the temperature at the middle level of the crust grows from the early beginning of the experiment (Figures 8a, 8b, and 8c). Later on, crustal shear zones develop in the lower crust (Figure 8). The thermomechanical processes associated to this localization of strain in the crust are complex and need a more through explanation (see below).

[25] The maximal plastic strain develops in wide zones of the upper crust located above the thickened parts of the crust (<35 km). The Moho boundary flattens due to the gravitational collapse of crustal structures favored by high-viscosity contrasts between the ductile crust and the competent mantle. The presence of a low-viscosity lower crust favors the development of hot intracrustal thermal anomalies laterally confined between competent mantle domains (Figures 7a–7c). At this early stage, no significant localization of strain occurs in the lower crust (see strain rate in Figure 7 (top)). In later stages, between 750 kyr and 1 Myr, remarkable strain rate contrasts develop in the lower crust (Figure 7, top). The amplitude ranges from maximum values of about 5×10^{-14} s^{-1} in a very localized area down to 10^{-17} s^{-1} anywhere else. The maximal strain rate zones, interpretable as shear zones, follow the 400°C isotherm, which roughly corresponds to the uppermost limit of the brittle-ductile transition in quartz assuming mean strain rate of 10^{-15} s^{-1}.

Figure 7. (opposite) (top) Strain rate in the crust; localization of strain in the lower crust. In the model, there is no localization in the lower crust before 1 Myr, and then differences develop. At 1.5 Myr, (a) the case with point A under crustal thickening leads to the formation of two symmetrical shear bands; (b) the case with point A under crustal thinning leads to the formation of only one shear band verging to the north at 1.5 Myr but at 2.5 Myr after the onset of rifting, a second shear band, symmetric to the first one, has formed, and (c) the case with a flat slab leads to the formation of two symmetrical shear bands at 1.5 Myr and after 2.5 Myr the shear band verging to the north seems to localize more strain then the other. (bottom) Plastic strain in the upper crust. The rest of the crust has been neglected because no brittle plastic deformation occurs deeper in the crust. (a), (b), and (c) Cases corresponding to the sketches presented in Figures 5a, 5b, and 5c. In all the cases, plastic strain first occurs on wide zones corresponding to the thick part of the crust and then localizes at the top of the ductile shear bands. See color version of this figure at back of this issue.

[26] The temperature curves (Figures 8a, 8b, and 8c) show that the temperature anomaly in the thickened part of the crust grows slowly until strain localization occurs in the lower crust (~750/1000 kyr). Then thermal advection accelerates leading to a concentration of high-temperature anomalies in zones of fastest vertical uplift (Figures 8d, 8e, and 8f). This acceleration is caused by positive feedback between the temperature, thermal buoyancy and effective viscosity of the material. One may note that in the initially thinned part of the crust, temperature decreases slowly since the degree of mechanical coupling between the crust and mantle (Figures 8a, 8b, and 8c) increases.

4.2. Mantle Control on Deformation

[27] Almost all effects and similarities described in the previous section refer to the particular initial crustal geometry. The mantle geometry affects the strain localization in the crust and particularly the symmetry of the computed rift structure and the vertical movements. Because the asthenosphere is less dense and hotter than the lithospheric slab and because the slab is retreating, upwelling of hot mantle material appears to be the main controlling factor. Significant convection in the asthenopheric mantle develops at the front of the slab for cases a and b. They influence the deformation style in the crust.

[28] In the case where the thickened crust occurs above point A, the upwelling mantle material reaches ~60 km depth within about 750 kyr and is located exactly beneath the zone affected by the collapse of the initially thickened crust. In this case, the hot thermal anomaly in the mantle and the intracrustal anomaly resulting from this collapse are vertically aligned (see temperature on Figure 6a). The resulting deformation in the crust is characterized by symmetrical repartition of strain into two shear zones (see strain rate Figure 7a, top). In the case of a flat slab (Figure 5c) the strain is also localized into two symmetrical shear zones (Figure 7c, top), but important differences from the previous model are observed at upper crustal scale. In the case of a flat slab, the intracrustal thermal anomaly grows earlier as the uplift is more efficient (see temperature curves at 5 km depth in Figures 8a and 8c for comparison). The second difference between the two profiles is the spatial distribution of vertical uplift: the amplitudes of the strain rates in the lower crust are rather close in both experiments, but the distribution is asymmetrical in the case of a flat slab (Figure 8f). This asymmetry is not present in case a (break point A situated beneath the thickened part of the crust). Heat flux from the mantle has an influence on the distribution of vertical uplift rates, but not on their maximum amplitudes.

[29] By contrast, in case b (point A shifted to the north of the thick part of the crust, Figure 5b), when strain localization begins in the lower crust, the hot thermal mantle upwelling is shifted to the north from the former collapsed zone (Figure 7b). This thermal horizontal gradient at the base of the collapsed zone favor strain localization on the north dipping potential shear zone (Figure 7b, top). In this case, the thermal anomaly is reduced compared with both the other cases.

[30] The experiments have been continued until 2.5 Myr after rifting. For cases a and c the results (not presented here) indicate no major change in the style of deformation, whereas case b was fairly more interesting. After, 2.5 Myr the slab has retreated. The thermal gradient at the base of the collapsed zone does not exist anymore and the asymmetric mode changes to a more symmetric one (Figure 7b, top).

5. Discussion

[31] The two main goals of our study were to characterize the mechanisms of strain localization in the crust in conditions similar to those observed in the Gulf of Corinth and to understand by this way the original aspect of the crustal structures observed in the gulf.

5.1. Mechanisms Leading to Strain Localization

[32] In all experiments, the strain localized in the brittle part of the crust and then propagated into the ductile part where an intracrustal thermal anomaly has been generated. A test made without thermal coupling indicates that no shear zone will ever occur if the thermal field remains constant in the crust. (Thermal state is fixed to the initial conditions. There is no anomaly forming during the collapse of the crust.) In this case plastic strain is less important than in the thermally coupled experiments. Using the thermomechanical approach, we can compute the development of the shear bands in the lower crust, which intensify and accelerate the plastic strain in the upper crust. As a result, our models predict two stages of evolution for the last million years in the Corinth rift. During the first stage, the area collapses, producing extension on a large regional scale, and causing normal faulting (Figure 9, step 1). Later, the thermal intracrustal anomaly produced in the crust during the collapse stage favors strain localization on symmetrical shear bands in the lower crust (Figure 9, step 2). These bands propagate downward from the center of the extensional zone and merge with the interface between the crust and the competent mantle in the zones of crust thinning inherited from the initial geometry (Figure 9, step 2).

[33] After the onset of the development of these bands, plastic strain becomes more intensive and tends to spatially localize in the brittle crust. This is the second phase during which the vertical movements are highest and the topography grows quickly.

[34] Our results suggest that the initial geometry of the crust can explain the existence of two phases of rifting without any change in the regional extension rate. Our experiments have shown that the geometry of the rift strongly depends on the position of the slab, which controls the symmetry, or asymmetry of the shear in the ductile crust (Figure 9, step 3).

5.2. Inferred Geodynamic Evolution of the Rift of Corinth

[35] The Gulf of Corinth is characterized by east–west contrasts in terms of the subsidence area and of the uplift and opening rate during the last million years. Westward

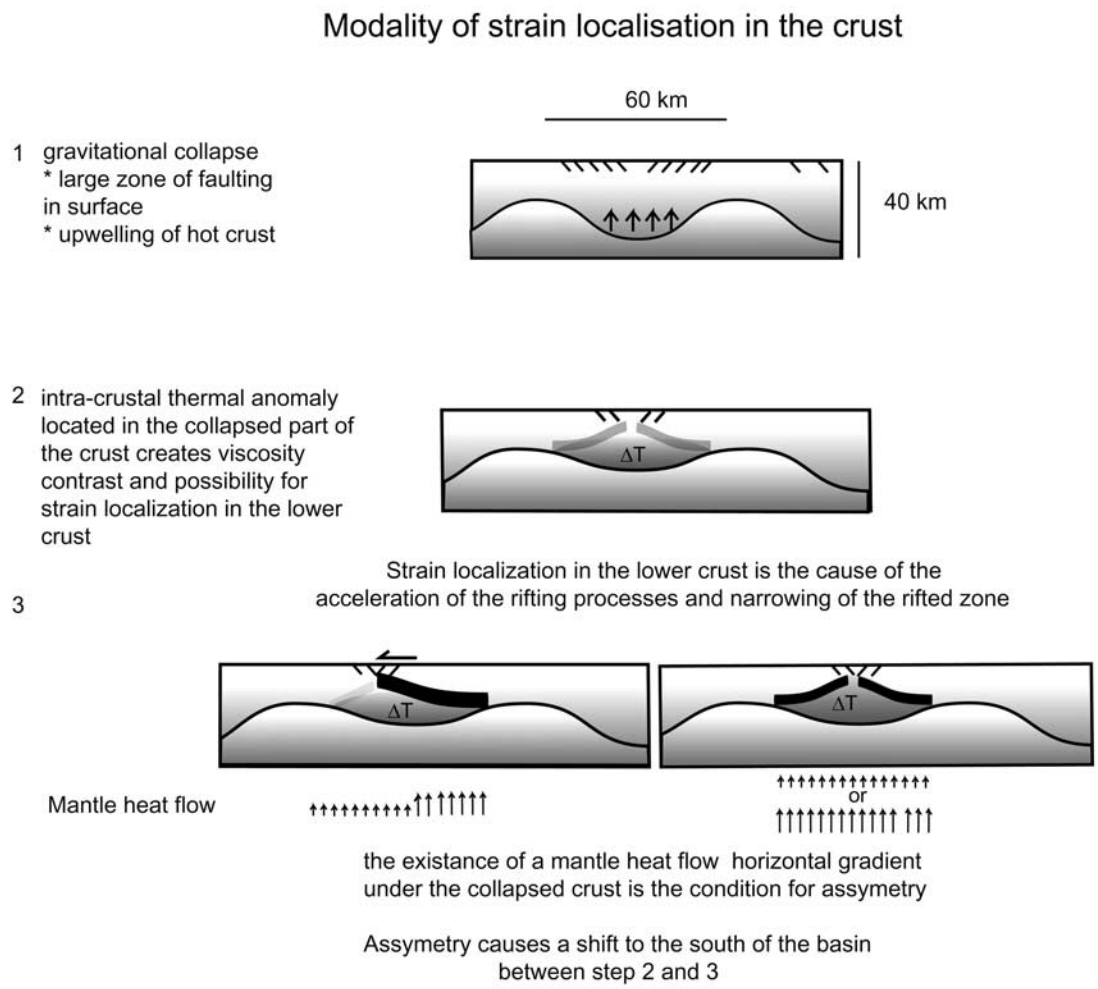

Figure 9. Strain localization in the crust: the role of initial thickness variation in a back arc domain context.

in the gulf, nearby the towns of Aigion and Xylocastro (profile 1 on Figure 10), the observations fit with case b (see Figure 5b) after 1 Myr. The model predicts the narrowing of the subsiding area and the increase of the differential uplift during the second stage (which has been also recorded on the sedimentary sequence by the change from alluvial fans to Gilbert's delta). During the second stage, the model predicts the development of the shear zone dipping to the north through the all lower crust from the depth of the brittle-ductile transition. This shear zone is compatible with the focal mechanism data of *Rigo et al.* [1996], which highlight a rotation of the *P* and *T* axes at the brittle-ductile transition depth. The model also predicts a progressive southward migration of the depocenter of the rift recorded on the Hellenic petroleum seismic data [*Clément*, 2000; *Moretti et al.*, 2002]. The current depocenter on profile 1 is located in the central part of the gulf.

[36] In the eastern part, the observations fit with case a 1 Myr after onset of rifting or case b after 2 Myr. Indeed, due to the slab retreat, this part of the rift has undergone various positions versus the slab since the beginning of the extension. On the second profile, normal faulting is active on both sides of the rift in the upper crust with faults dipping both northward and southward sometimes affected by the same seismic crisis like in 1981 [*Jackson et al.*, 1982]. These observations clearly correlate with the results of case a at 1 Myr and of case b at 2 Myr. However, only case b can explain the migration of the depocenter in the southward direction observed in the marine seismic data.

6. Conclusion

[37] The area of the Gulf of Corinth presents inherited crustal thickness undulations as well as strong lateral variations in mantle heat flux. Our approach consisted in testing three different initial geometries corresponding to the three main possible spatial relationship between the high heat flux at the front of the subducting Hellenic slab

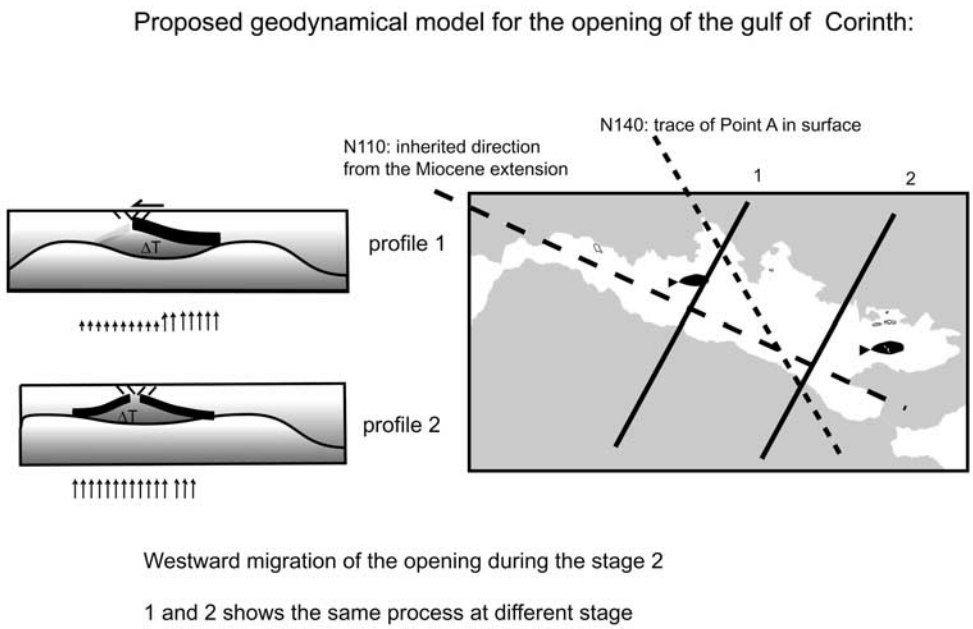

Figure 10. Proposed geodynamical model for the opening of the Gulf of Corinth.

and the thickened crust beneath the Gulf of Corinth. We have thus been able to propose a single model for the opening of the gulf of Corinth in which all observations made from west to east are well related to different stages of evolution in case b (i.e., case with thermal anomaly shifted to the north from the thickened crustal zone). Thus east–west variations in the Gulf of Corinth can be explained by the slab retreat and by the difference between the dipping direction of the slab (N50°) and the direction of the inherited crustal structures (N120°) in the area (Figure 10). In all of the studied profiles (Figure 10), the rifting begins from collapse of the crust structures. On profile 1, the evolution is stopped at this stage. In the center of the Gulf of Corinth, the present situation corresponds to the asymmetric stage (case b after 1 Myr) whereas the eastern profile corresponds to case b after 2 Myr (or case a after 1 Myr).

[38] In the brittle upper crust, the fault geometries are mainly due to the far stress field while in the lower crust and upper mantle, the interactions between the mantellic flow and the regional stress field lead to more complex coupling. At such a depth, the contrasts in the mechanical behavior play a major role in reorientation of the stress field and in strain localization. Our model does not suggest a propagation of the asymmetric shear bands through the upper crust.

Appendix A: Numerical Model

[39] The 2-D numerical scheme was developed from the PARAVOZ code [*Poliakov et al.*, 1993] based on the FLAC algorithm [*Cundall*, 1989]. The PARAVOZ code is a fully explicit time-marching large-strain Lagrangian algorithm that solves the full Newtonian equations of motion

$$\rho \frac{\partial}{\partial t}\left(\frac{\partial \mathbf{u}}{\partial t}\right) - \mathrm{div}\ \sigma - \rho \mathbf{g} = 0$$

coupled with constitutive equations of kind:

$$\frac{D\sigma}{Dt} = F\left(\sigma, \mathbf{u}, \nabla \frac{\partial \mathbf{u}}{\partial t}, \ldots T \ldots\right)$$

and with those of heat transfer (diffusion and advection):

$$\rho C_p \partial T/\partial t + \mathbf{u}\nabla T - \mathrm{div}(\mathbf{k}\nabla T) - H_r = 0$$

and surface erosion (linear or nonlinear diffusion):

$$\partial h_s/\partial t - \nabla(k_e \nabla h_s) = 0,$$

where $\mathbf{u}$, $\boldsymbol{\sigma}$, $\mathbf{g}$, $\mathbf{k}$ are the respective vector-matrix terms for the displacement, stress, acceleration due to body forces and thermal conductivity. The scalar terms t, ρ, C_p, T, H_r, h_s, k_e respectively designate time, density, specific heat, temperature, internal heat production, surface elevation and coefficient of erosion. The terms $\partial/\partial t$, D/Dt, F denote a time derivative, an objective time derivative and a functional, respectively.

[40] In the numerical scheme, a solution of the equations of motion provides velocities at mesh points, which allows calculation of element strains. These strains are used in the

constitutive relations to calculate element stresses and equivalent forces, which form the basic input for the next calculation cycle. The Lagrangian coordinate mesh moves with the material, and at each time step the new positions of the mesh grid nodes are calculated and updated in large strain mode from the current velocity field using an explicit procedure (two-stage Runge-Kutta). To solve explicitly the governing equations, the PARAVOZ (FLAC) method uses a dynamic relaxation technique by introducing artificial masses in the inertial system. An adaptive remeshing technique developed by *Poliakov et al.* [1993] allows resolution of strain localizations leading to formation of the faults. The solver of the FLAC method does not imply any inherent rheology assumptions, in contrast with the most common finite element techniques based on the implicit displacement method. The main interest in this method thus refers to its capability to model physically highly unstable processes and handle strongly nonlinear rock rheologies in their explicit form of the constitutive relationship between strain and stress.

A1. Brittle-Ductile Interactions

[41] The ductile-elastic-brittle rheology used here (as well as in most geodynamic codes) can be schematically represented as a serial connection of an elastic string component, frictional block component and a nonlinear viscous dash-pot component. The total incremental strain in such a system is a sum of incremental viscous, plastic and elastic strains in each of the components, whereas the steady state component stresses are equal. On each time step, the algorithm uses a current solution for strain and strain rate in each numerical element to predict incremental stress in each of the rheological components for the next time step. The component which predicts lowest stress for given strain will dominate the overall behavior of the grid element. Exact constitutive relations for each component are solved on each time step, which makes the algorithm very robust. The behavior of each rheological component plugged in a chain may be completely different from its stand-alone behavior. For example, pure viscous deformation does not depend on strain, but in elastoviscous material, the initial strain controls the viscous stress and strain rate. In a serial viscoplastic media, the plastic stress limits the viscous stress (and vice versa), and consequently the viscous strain rate. Thus a plastic component, which alone is strain rate independent, controls, and is being controlled by, the strain rate in a viscoplastic couple. For this reason, in the vicinity of the brittle-ductile transition, the velocity field in both ductile and brittle zones is strongly controlled by the behavior of all ductile, brittle and elastic parts. This behavior cannot be reduced to that of a viscous or viscoelastic material.

[42] The algorithm handles nonlinear plastic-elastic-viscous behavior allowing for realistic representations of rock rheology. Brittle deformation is approximated by a Mohr-Coulomb plasticity term; Hooke's law approximates the elastic term. This formulation corresponds to a non-associated elastoplasticity. Intracrystalline plasticity, which corresponds to effectively nonlinear viscous behavior, is approximated by ductile creep law derived from the data of experimental rock mechanics. According to this law, the strain rate is a nonlinear function of the deviatoric stress and is an exponential function of the inverse temperature. The corresponding constitutive behavior can be schematically represented as a serial connection of an elastic spring, of a viscous dashpot and of a frictional block.

A2. Plastic (Brittle) Behavior

[43] The brittle behavior of the uppermost lithosphere is given by experimentally derived Byerlee's law [*Byerlee*, 1978]:

$$\tau \approx 0.85\sigma_n, \quad \sigma_n < 200 \text{ MPa},$$

$$\tau \approx 0.5\text{MPa} + 0.6\sigma_n, \quad \sigma_n > 200 \text{ MPa},$$

or

$$\sigma_1 - \sigma_3 \approx 4\sigma_3, \quad \sigma_3 < 110 \text{ MPa},$$

$$\sigma_1 - \sigma_3 \approx 2.1\sigma_3 + 210, \quad \sigma_3 > 110 \text{ MPa},$$

where τ is shear stress and σ_n' is effective normal stress, σ_1 and σ_3 are principal stresses. Byerlee's law corresponds to pressure dependent Mohr-Coulomb material with friction angle ϕ and cohesion $|C_0|$ [e.g., *Gerbault et al.*, 1999]:

$$|\tau| = C_0 - \tan\phi\sigma_n', \tag{A1}$$

where σ_n is normal stress $\sigma_n = P + \sigma_{II}^{dev} \sin\phi$, P is the effective pressure, σ_{II}^{dev} is the second invariant of deviatoric stress, or effective shear stress. The Condition of transition to brittle deformation (function of rupture f) freads as $f = \sigma_{II}^{dev} + P \sin\phi - C_0 \cos\phi = 0$ and $\partial f/\partial t = 0$. In terms of principal stresses, the equivalent of the yield criterion (A1) reads as

$$\sigma_1 - \sigma_3 = -\sin\phi\left(\sigma_1 + \sigma_3 - 2C_0 \tan^{-1}\phi\right) \tag{A2}$$

Parameters ϕ = 30°–33° and $|C_0|$ = 5–20 MPa represent Byerlee's law for most rocks. In case of important fluid pressure, which is the normal case for oceanic crust, σ_n is reduced to $\sigma'_n = \sigma_n - P_f$, where P_f is fluid pressure.

A3. Elastic Behavior

[44] The elastic part is defined using commonly inferred values of elastic constants for lithospheric rocks, that is, with Young's modulus of 80 GPa and Poisson's ratio of 0.25 [*Turcotte and Schubert*, 1982]:

$$\sigma_{ik} = \left(\lambda + 2\mu 3^{-1}\right)\varepsilon_{ll}\delta_{ik} + 2\mu\left(\varepsilon_{ik} - 3^{-1}\varepsilon_{ll}\delta_{ik}\right), \tag{A3}$$

where λ and μ are Lamé's constants related to Young's modulus, E, and Poissons' ratio, υ, as $\lambda = E\upsilon[(1 + \upsilon)(1-2\upsilon)]^{-1}$; $\mu = E[2(1 + \upsilon)]^{-1}$, and δ is Kronecker's delta.

A4. Viscous (Ductile) Behavior

[45] A non-Newtonian ductile rheology is presented by a power law stress and exponential temperature dependence of the strain rate:

$$\dot{\varepsilon} = A(\sigma_1 - \sigma_3)^n \exp - \frac{Q}{RT}, \tag{A4}$$

where the parameters A, n, Q are experimentally determined material constants, and are the principal stresses, is the strain rate, T is the absolute temperature, and R is the universal gas constant. The material parameters for the creep law are given in Table 2. The creep law allows us to estimate the effective (instantaneous) viscosity of the rock. According to this law, in the upper mantle just below the lithosphere, viscosity is about 10^{19} Pa s, which matches the values obtained from postglacial rebound data [*Turcotte and Schubert*, 1982]; in the depth interval from 50 to 0 km it increases from 10^{19} to 10^{25}–10^{27} Pa s.

[46] **Acknowledgments.** Thanks to Badr Ghorbal for the microstructural results. We thank L. Jolivet, C. Tiberi and F. Gueydan for constructive discussions. Thanks to R. H. Gabrielsen and an anonymous reviewer for their advice and corrections and to Alex Poliakov for the time he spent too. This work has been done in relation with the Corinth rift laboratory development. Additional information: http://www.ifp.fr/corinth and http://www.corinth-rift-lab.org.

References

Armijo, R., B. Meyer, G. C. P. King, A. Rigo, and Papanastassiou, Quaternary evolution of the Corinth rift and its implications for the late Cenozoic evolution of the Aegean, *Geophys. J. Int.*, *126*, 11–53, 1996.

Aubouin, J., et al., Contribution à la géologie des Hellènides: Le Gavrovo, le Pinde et la zone ophiolitique subpélagonienne, *Ann. Soc. Geol. Nord*, *90*, 277–306, 1970.

Briole, P., A. H. Lyon Caen, J. Ruegg, K. Papazissi, C. Mistakaki, A. Balodimou, G. Veis, D. Hatzfeld, and A. Deschamps, Active deformation, of the gulf of Korinthos, Greece: Results from repeated GPS surveys between 1990 and 1995, *J. Geophys. Res.*, *105*, 25,605–25,625, 1999.

Burov, E. B., and M. Diament, The effective elastic thickness (T_e) of continental lithosphere: What does it really mean?, *J. Geophys. Res.*, *100*, 3905–3927, 1995.

Burov, E. B., and A. N. B. Poliakov, Erosion and rheology controls on syn-and post-rift evolution: Verifying old and new ideas using a fully coupled numerical model, *J. Geophys. Res.*, *106*, 16,461–16,481, 2001.

Byerlee, J., Friction of rocks, *Pure Appl. Geophys.*, *116*, 615–626, 1978.

Clément, C., Imagerie sismique crustale de la subduction Hellénique et du golfe de Corinthe, Univ. Paris VII, Paris, 2000.

Cundall, P. A., Numerical experiments on localization in frictional materials, *Ing. Arch.*, *59*, 148–159, 1989.

Fytikas, M. D., and N. P. Kolios, Preliminary heatflow-map of Greece, in *Terrestial Heatflow in Europe*, edited by V. Cermak and L. Rybach, pp. 197–205, Springer-Verlag, New York, 1979.

Gautier, P., and J. P. Brun, Crustal scale geometry and kinematiks of late orogenic extension in the central aegean (Cyclades, Evvia Island), *Tectonophysics*, *238*, 399–424, 1994.

Gautier, P., J. P. Brun, R. Moriceau, D. Sokoutis, J. Martinod, and L. Jolivet, Timing, kinematics and cause of the Aegean extension: A scenario based on a comparison with simple analogues experiments, *Tectonophysics*, *315*, 31–72, 1999.

Gerbault, M., E. B. Burov, A. N. B. Poliakov, and M. Daignières, Do faults trigger folding in the lithosphere?, *Geophys. Res. Lett.*, *26*, 271–274, 1999.

Ghisetti, F. C., L. Vezzani, F. Agosta, R. Sibson, and I. Moretti, Tectonic setting and sedimentary evolution of the south-west margin of the Corinth rift (Aigion-Xylocastro area), Inst. Fr. du Pétrole, Rueil Malmaison, France, 2001.

Ghorbal, B., Quels arguments en faveur d'un détachement Plio-Quaternaire au sud du Golfe de Corinthe?: Etudes tectono-métamorphique des Phyllades du Péloponnèse septentrionnal., mémoire de DEA, Univ. Paris VI, Paris, 2002.

Jackson, J. A., J. Gagnepain, G. Houseman, G. C. P. King, P. Papadimitriou, C. Soufleris, and J. Virieux, Seismicity, normal faulting and the geomorphological development of the gulf of Corinth (Greece): The Corinth earthquakes of February and March 981, *Earth Planet. Sci. Lett.*, *57*, 377–397, 1982.

Jacobshagen, V., S. Duerr, F. Kockel, K. Kopp, and G. Kowalczyk, Structure and geodynamic Evolution of the Aegean Region, in *Alps Apennines Hellenides: Geodynamic Investigations Along Geotraverses by an International Group of Geoscientists*, *Inter-Union Comm. Geodyn. Sci. Rep.*, *38*, pp. 537–620, E. Schweizerbart'che, Stuttgart, Germany, 1978.

Jolivet, L., A comparison of geodetic and finite strain pattern in the Aegean, geodynamic implications, *Earth Planet. Sci. Lett.*, *187*, 95–104, 2001.

Jolivet, L., J. P. Brun, P. Gautier, S. Lallemant, and M. Patriat, 3D kinematics of extension in the Aegean region from the early Miocene to the present, insights from the ductile crust, *Bul. Soc. Geol. Fr.*, *165*, 195–209, 1994.

Lavier, L. L., W. R. Buck, and A. N. B. Poliakov, Self consistent rolling hinge model for the evolution of large offset low-angle faults, *Geology*, *27*, 1127–1130, 1999.

Lyon Caen, H., K. Makopoulos, P. Papadimitriou, A. Deschamps, P. Bernard, F. Pachianni, S. Bourouis, H. Castarede, and F. Cornet, Seismicity in the Aigion area as seen by the Corinth Rift seismological network, *Geophys. Res. Abstr.* [CD-ROM], *4*, EGS02-A-05400, 2002.

McKenzie, D., Active tectonics of the mediteranean region, *Geophys. J. R. Astron. Soc.*, *30*, 109–185, 1972.

Micarelli, L., J. M. Daniel, and I. Moretti, Structural characterisation of Quaternary fault zones in the Aigion area (Greece), *Geophys. Res. Abstr.* [CD-ROM], *4*, EGS02-A-02728, 2002.

Moretti, I., F. Ghisetti, L. Vezani, and R. Sibson, Tectonic setting and sedimentary evolution of the south-west margin of the Corinth Rift (Aigion-Xylocastro area), *Geophys. Res. Abstr.* [CD-ROM], *4*, EGS02-A-02906, 2002.

Ori, G. G., Geological hystory of the extensional basin of the gulf of Corinth (Miocene Pleistocene), Greece, *Geology*, *17*, 918–921, 1989.

Pantosti, D., P. M. De Martini, D. Papanastassiou, N. Palyvos, F. Lemeille, and G. Stavrakakis, A reappraisal of the 1894 Atlantic earthquake surface ruptures, central Greece, *Bull. Seismol. Soc. Am.*, *91*, 760–780, 2001.

Poliakov, A. N. B., and W. R. Buck, Faulting due to stretching of visco-elastic-plastic lithosphere: Some remarks on brittle-ductile transition, rift shoulders and depth of necking, *Eos Trans. AGU*, *77*(46), Fall Meet. Suppl., F702, 1996.

Poliakov, A. N. B., Y. Y. Podladchikov, and C. Talbot, Initiation of salt diapirs with frictional overburden: Numerical experiments, *Tectonophysics*, *228*, 199–210, 1993.

Rigo, A., H. Lyon-Caen, R. Armijo, A. Deschamps, D. Hatzfeld, K. Makropoulos, and K. I. Papadimitriou, A microseismic study in the western part of the Gulf of Corinth (Greece) implications for large-scale normal faulting mechanisms, *Geophys. J. Int.*, *126*, 663–688, 1996.

Sorel, D., A Pleistocene and still active detachment fault and the origin of Corinth Patras Rift, Greece, *Geology*, *28*, 83–86, 2000.

Spakman, W., M. J. R. Wortel, and N. J. Vlaar, The Hellenic subduction zone: A tomographic image and its geodynamic implications, *Phys. Earth Planet. Inter.*, *79*, 3–74, 1988.

Stefatos, A., G. Papatheodorou, G. Ferentinos, M. R. Leeder, and R. E. L. Collier, Seismic reflection imaging of active offshore faults in the Gulf of Corinth, *Geophys. Res. Abstr.* [CD-ROM], *4*, 2002a.

Stefatos, A., G. Papatheodorou, G. Ferentinos, M. R. Leeder, and R. E. L. Collier, Seismic reflection imaging of active offshore faults in the Gulf of Corinth; their seismotectonic significance, *Basin Res.*, *14*, 487–502, 2002b.

Tibéri, C., Rift de Corinthe et d'Evvia (Grèce): Structure lithosphérique par tomographie télésismique et gravimétrie, thèse de 3ième cycle thesis, 239 pp., Univ. Paris VII, Paris, 2000.

Trotet, F., Exhumation des roches de Haute Pression-Basse Température le long d'un transect des Cyclades au Péloponnèse (Grèce): Implications Géodynamiques, Univ. Paris XI, Paris, 2000.

Turcotte, D. L., and G. Schubert, *Geodynamics: Applications of Continuum Physics to Geological Problems*, 450 pp., John Wiley, New York, 1982.

Wernicke, B., Low angle normal faults in the Basin and Range province: Nappe tectonics in an extending orogen, *Nature*, *291*, 645–648, 1981.

Xypolias, P., and T. Doustos, Kinematics of rocks flow in a crustal-scale shear zone: Implication for the orogenic evolution of the south-western Hellenides, *Geol. Mag.*, *137*, 81–96, 2000.

E. Burov and L. Le Pourhiet, Laboratoire de Tectonique, Université Pierre et Marie Curie, 4 place Jussieu, F-75252 Paris Cedex 05, France. (laetitia.lepourhiet@lgs.jussieu.fr)

I. Moretti, Institut Français du Pétrole, 1-4, avenue de Bois Préau, F-92852 Rueil Malmaison, France.

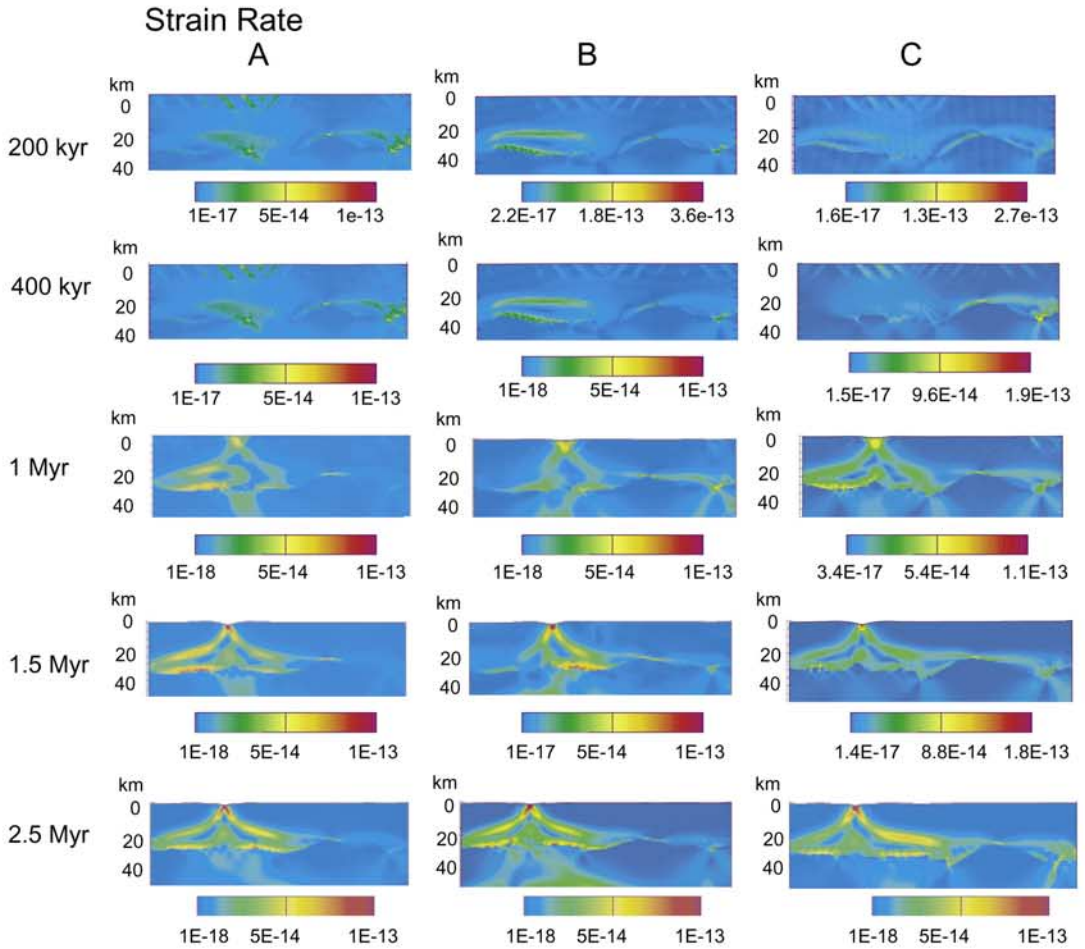
Strain Rate
A
B
C
200 kyr
400 kyr
1 Myr
1.5 Myr
2.5 Myr
km
0
20
40
1E-17 5E-14 1e-13
2.2E-17 1.8E-13 3.6e-13
1.6E-17 1.3E-13 2.7e-13
1E-17 5E-14 1E-13
1E-18 5E-14 1E-13
1.5E-17 9.6E-14 1.9E-13
1E-18 5E-14 1E-13
1E-18 5E-14 1E-13
3.4E-17 5.4E-14 1.1E-13
1E-18 5E-14 1E-13
1E-17 5E-14 1E-13
1.4E-17 8.8E-14 1.8E-13
1E-18 5E-14 1E-13
1E-18 5E-14 1E-13
1E-18 5E-14 1E-13

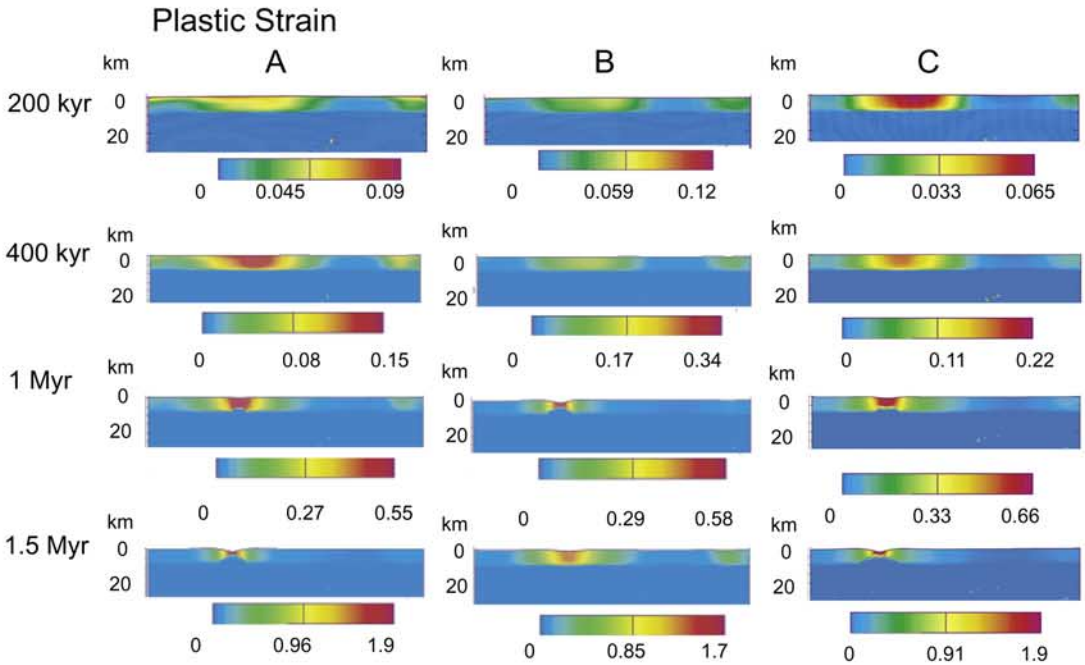
Plastic Strain
A
B
C
200 kyr
400 kyr
1 Myr
1.5 Myr
km
0
20
0 0.045 0.09
0 0.059 0.12
0 0.033 0.065
0 0.08 0.15
0 0.17 0.34
0 0.11 0.22
0 0.27 0.55
0 0.29 0.58
0 0.33 0.66
0 0.96 1.9
0 0.85 1.7
0 0.91 1.9

Figure 7. (opposite) (top) Strain rate in the crust; localization of strain in the lower crust. In the model, there is no localization in the lower crust before 1 Myr, and then differences develop. At 1.5 Myr, (a) the case with point A under crustal thickening leads to the formation of two symmetrical shear bands; (b) the case with point A under crustal thinning leads to the formation of only one shear band verging to the north at 1.5 Myr but at 2.5 Myr after the onset of rifting, a second shear band, symmetric to the first one, has formed, and (c) the case with a flat slab leads to the formation of two symmetrical shear bands at 1.5 Myr and after 2.5 Myr the shear band verging to the north seems to localize more strain then the other. (bottom) Plastic strain in the upper crust. The rest of the crust has been neglected because no brittle plastic deformation occurs deeper in the crust. (a), (b), and (c) Cases corresponding to the sketches presented in Figures 5a, 5b, and 5c. In all the cases, plastic strain first occurs on wide zones corresponding to the thick part of the crust and then localizes at the top of the ductile shear bands.